Military Technical College
Kobry El-Kobbah,
Cairo, Egypt.

17th International Conference on Applied Mechanics and Mechanical Engineering.

FINITE ELEMENT SIMULATION OF ELASTIC AND QUASI – STATIC CRACK PROPAGATION UNDER MIXED MODE LOADING CONDITIONS

S. A. K. Yossif*

ABSTRACT

This paper employs the classical finite element method in simulation of crack propagation problems in a linear elastic and isotropic medium under mixed loading conditions. Two crack problems are considered; an inclined edge crack in a plate under tensile loading, and a shifted crack in a beam under three - point bending loading. The critical energy release rate criterion determines the threshold of propagation. The maximum tangential stress criterion determines the direction of crack propagation. Strain energy release rates are calculated using the virtual crack closure technique (VCCT). Deformation field is plane strain. The crack tip region is meshed with non-singular 8-noded isoparametric quadrilateral elements. Realization of all numerical computations and demonstration of results are completely composed and written in MATLAB language. Results showed acceptable accuracy when compared with analytical ones, experimental work and those obtained by commercial ANSYS APDL program.

KEY WORDS

Crack propagation, virtual crack closure technique, mixed mode loading, crack path detection, maximum tangential stress criterion, and finite element method.

* Lecturer at Mechanical Design Department – Faculty of Engineering – Mataria – Helwan University – Cairo – Egypt. Email: salah.aleasha@hotmail.com.

NOMENCLATURE

a	Crack length.	K_{eq}	Equivalent stress intensity factor of the initial crack.
a_c	Critical crack length.	$K_I^{\theta_c}$	Equivalent stress intensity factor of the propagated crack.
Δa	Incremental crack length.	K	Element stiffness matrix.
D	Elasticity matrix.	N	Matrix of shape functions.
d	Element nodal displacement vector.	P_y	Applied concentrated load in y- direction.
E	Young's modulus.	T_y	Applied surface traction in y-direction.
E'	Effective Young's modulus.	(t, n)	Local normal and tangential coordinate system.
e_{K_I}	Percentage error in computation of K_I.	(x, y)	Local Cartesian coordinate system.
F	Element force vector.	ν	Poisson's ratio.
F_x and F_y	Nodal forces in x- and y-directions respectively.	$\boldsymbol{\sigma}$, and $\boldsymbol{\varepsilon}$	Element Cartesian stress and strain vectors.
G_I, G_{II}, and G_T	Mode I, Mode II and total strain energy release rates.	σ_r, σ_θ, and $\tau_{r\theta}$	Radial, tangential and shear stresses in polar coordinates system.
G_{Ic}, G_{IIc}, and G_{Tc}	Critical values of G_I, G_{II}, and G_T.	σ_{yp}	Material yield point.
K_I and K_{II}	Mode I and II stress intensity factors.	θ_c	Crack deflection angle.
K_{Ic}	Fracture toughness.	Δ	Length of an element edge.
u, and v	Displacement fields in x- and y- directions, respectively.	δ^t and δ^n	Nodal displacements in t- and n- directions, respectively.

ABBREVIATION

FEM	Finite element method.	$VCCT$	Virtual crack closure technique.
$LEFM$	Linear elastic fracture mechanics.	Q8	Eight-noded isoparametric quadrilateral element.
SIF	Stress intensity factor.		

INTRODUCTION

In the framework of the finite element method, simulation of crack propagation is possible [1-2]. Crack propagation is a moving singularity problem [3]. Strain and stress fields around crack tip are singular [4]. Two problems arise; modeling singularity around the crack tip and creation of new crack surfaces as the crack tip advances. Special family of high order finite elements was developed to implement stress singularities in the vicinity of the crack tip [5]. They were called singular elements.

None-corner nodes of a singular element are displaced from their regular positions towards corner nodes which are meshing the crack tip. In case of eight-noded isoparametric quadrilateral element (Q8), the amount of this shift is the quarter length of an element edge. Creation of new crack surfaces necessitates simultaneous re-meshing of the continuum with every increment of the propagated crack. The extended finite element method (X-FEM) is one of the recent numerical methods that overcome the problem of re-meshing [6-7].

This paper deals with the numerical simulation of the crack propagation problem in a linear and elastic medium under mixed loading conditions. The inertia forces are neglected so crack propagation is considered as a quasi - static. Two crack problems are considered; the first is an inclined edge crack in a finite plane under tensile loading, and the second is a shifted crack in a beam under three-point bending loading. Both cracks are under mixed loading conditions; i.e. opening and shearing or sliding modes. Tearing mode is not considered in this work. For a crack to propagate, it should satisfy a fracture criterion and select a direction for its propagation. The simple fracture criterion [8] determines the threshold of propagation. Besides, the maximum tangential stress criterion defines the direction of crack propagation [9]. Strain energy release rates are calculated using the virtual crack closure technique (VCCT) [10]. The stress intensity factors (SIFs) are calculated as functions of strain energy release rates [11].

In this work, propagation direction of each crack problem is invariant. A crack neither bifurcates nor branches. A crack either advances or arrests; depending on whether the fracture criterion is exceeded or not. Thus, simulation of crack propagation doesn't require simultaneous re-meshing with every crack increment. Accordingly, each crack problem is meshed twice. The first mesh is used to calculate the initial crack characteristics and the crack deflection angle. Crack deflection angle is the acute angle between the initial crack and the expected path of its propagation. Before re-meshing, the propagation path is laid on the initial model as a line emanating from the crack tip and oriented to the initial crack by the calculated crack deflection angel. The second mesh, while discretizing the main model, aims to divide the crack path into a number of structured Q8 elements. Each element edge on the path represents an amount of a crack increment if the fracture criterion is satisfied. For every increment of the crack, all crack characteristics are calculated and compared with fracture criterion to determine whether the crack would advance or arrest.

To model the creation of new crack faces corresponding to a crack increment, the element nodes on the crack path are duplicated and elements connectivity matrix are changed accordingly to decouple the two adjacent element on the both sides of the crack path and allow the motion of the crack tip. This procedure is accompanied by continuous update of nodal coordinates, element stiffness matrices and global force vector. Deformation field is assumed to be a plane strain. The classical displacement-based finite element method is used to calculate deformation, strain and stress fields [12-13]. The model is meshed with eight-noded isoparametric quadrilateral elements (Q8). The crack tip region is meshed with non-singular (Q8) elements. The mesh of non-singular Q8 elements is too dense to compensate the singularity of stress fields around crack tip.

Realization of all numerical computations and demonstration of results are completely composed and written in MATLAB® language. Meshing the computational domains

and crack tip region are performed by a free downloadable program; AUTOMESH-2D [14]. The AUTOMESH-2D generates quadrilateral four – noded elements (Q4). Transformation from Q4 to Q8 elements is performed by a special function written in MATLAB language. To verify the correctness of the written program, the results of SIFs in case of the single edge notch test specimen and the three – point bend test specimen are compared with analytical ones. In addition, the results of SIFs are compared with those obtained by the commercial ANSYS APDL program. Moreover, the results of propagation of the shifted crack in John and Shah beam are compared with their experimental work and the theoretical work of Rabczuk and Belytscho [15].

STRESS FIELD AROUND THE CRACK TIP

According to [4], stress fields around a crack tip are singular. Taking the crack tip as an origin of a local polar coordinates system (r, θ), Fig. 1, the expressions of radial σ_r, tangential σ_θ, and shear stress $\tau_{r\theta}$ are written as the following:

$$\sigma_r = \frac{K_I}{\sqrt{2\pi r}}\left\{\cos\left(\frac{\theta}{2}\right)\left[1+\sin^2\left(\frac{\theta}{2}\right)\right]\right\} + \frac{K_{II}}{\sqrt{2\pi r}}\left\{\sin\left(\frac{\theta}{2}\right)\left[1-3\sin^2\left(\frac{\theta}{2}\right)\right]\right\} \quad (1.a)$$

$$\sigma_\theta = \frac{K_I}{\sqrt{2\pi r}}\cos^3\left(\frac{\theta}{2}\right) - 3\frac{K_{II}}{\sqrt{2\pi r}}\sin\left(\frac{\theta}{2}\right)\cos^2\left(\frac{\theta}{2}\right) \quad (1.b)$$

$$\tau_{r\theta} = \frac{K_I}{\sqrt{2\pi r}}\sin\left(\frac{\theta}{2}\right)\cos^2\left(\frac{\theta}{2}\right) + \frac{K_{II}}{\sqrt{2\pi r}}\left\{\cos\left(\frac{\theta}{2}\right)\left[1-3\sin^2\left(\frac{\theta}{2}\right)\right]\right\} \quad (1.c)$$

Where K_I and K_{II} are stress intensity factors (SIF) corresponding to opening and shearing modes respectively. They measure the severity of stress fields in the vicinity of crack tip, [11].

FRACTURE CRITERIA

Under mixed loading mode, crack propagates if a fracture criterion is satisfied. Reeder [8] proposed simple, linear, bilinear, power law, exponential Hackle, exponential $\frac{K_I}{K_{II}}$ and interaction criteria. In this work, the simple criterion is selected to govern the onset of crack propagation. According to the simple criterion, the crack starts to grow when:

$$G_I = G_{Ic} \qquad G_{II} = G_{IIc} \qquad G_I + G_{II} = G_T = G_{Tc} \quad (2.a, b, c)$$

The energy release rate is related to SIF according to the following relations, [9]:

$$G_I = \frac{K_I^2}{E'} \qquad G_{II} = \frac{K_{II}^2}{E'} \quad (3.a, b)$$

Analogically to equations (3), it may be convenient to consider the concept of the equivalent SIF in case of the mixed mode condition as the following:

$$G_T = \frac{K_{eq}^2}{E'} \qquad K_{eq} = \sqrt{K_I^2 + K_{II}^2} \qquad \text{(4.a, b)}$$

By investigation of equations (2), the simple criterion of fraction may be rewritten in terms of fracture toughness of the material K_{Ic} as the following:

$$K_{eq} = K_{Ic} \qquad K_I^2 + K_{II}^2 = K_{Ic}^2 \qquad \text{(5.a, b)}$$

In the present work, equations (5) are considered as a threshold criterion for crack propagation, because the fracture toughness K_{Ic} is abundantly tabulated in material's data book [16].

MAXIMUM TANGENTIAL STRESS CRITERION

If the fracture criterion was exceeded, the crack would propagate. According to the criterion of maximum tangential stress [4, 9], crack would propagate along the direction perpendicular to that of maximum tangential stress. The direction of crack path is determined by defining the crack deflection angle; θ_c, as shown in Fig. 2. The angle θ_c represents the angular position of plane where shear stress is zero. It is calculated by nullifying the equation of shear stress, equation (1.c), and considering the condition of maximizing the equation of tangential stress, equation (1.b). Thus, conditions of numerical computations of the direction of crack propagation are:

$$K_I \sin\theta_c + K_{II}(3\cos\theta_c - 1) = 0 \qquad \left.\frac{\partial^2 \sigma_\theta}{\partial \theta^2}\right|_{\theta=\theta_c} < 0 \qquad \text{(6.a, b)}$$

Maximum tangential stress at the crack deflection angle is:

$$\sigma_\theta^{max} = \frac{1}{\sqrt{2\pi r}} \left[K_I \cos^3\left(\frac{\theta_c}{2}\right) - 3K_{II} \sin\left(\frac{\theta_c}{2}\right)\cos^2\left(\frac{\theta_c}{2}\right)\right] \qquad \text{(7.a)}$$

If the value of radial stress at crack deflection angle; i.e. $\sigma_r(\theta_c)$ is small compared to σ_θ^{max}, the equivalent SIF of the propagated crack would be calculated as the following, see Fig. 2:

$$K_I^{\theta_c} = \sigma_\theta^{max}\sqrt{2\pi r} \qquad \text{(7.b)}$$

By substituting of equation (7.a) into (7.b), the $K_I^{\theta_c}$ is related to K_I and K_{II} by the following equation [9]:

$$K_I^{\theta_c} = K_I \cos^3\left(\frac{\theta_c}{2}\right) - 3K_{II} \sin\left(\frac{\theta_c}{2}\right) \cos^2\left(\frac{\theta_c}{2}\right) \quad (7.c)$$

The propagating crack still advances as long as the value of $K_I^{\theta_c}$ is larger than or equal to the fracture toughness of the material. Thus, the condition of crack arrest is:

$$K_I^{\theta_c} < K_{I_c} \quad (8)$$

THE PRINCIPAL OF VIRTUAL CRACK CLOSURE TECHNIQUE (VCCT)

According to Raju [5], the energy release rates in case of non-singular eight – noded quadrilateral isoparametric element (Q8) are calculated according to the following equations:

$$G_I = -\frac{1}{2\Delta}\left[F_{y_i}(v_m - v_{m'}) + F_{y_j}(v_l - v_{l'})\right] \quad (9.a)$$

$$G_{II} = -\frac{1}{2\Delta}\left[F_{x_i}(u_m - u_{m'}) + F_{x_j}(u_l - u_{l'})\right] \quad (9.b)$$

It should be noted that, edges of elements I, J, I' and J' should be perpendicular to the direction of crack extension. Hence, in case of inclined crack as shown in Fig. 3(b), a local (t, n) coordinate system should be fixed at the crack tip i. The t- axis in the direction of crack extension, and n- axis is perpendicular to it. In case of an inclined crack, expressions of strain energy release rates are written as the following:

$$G_I = -\frac{1}{2\Delta}\left[F_{n_i}\left(\delta_m^n - \delta_{m'}^n\right) + F_{n_j}\left(\delta_l^n - \delta_{l'}^n\right)\right] \quad (10.a)$$

$$G_{II} = -\frac{1}{2\Delta}\left[F_{t_i}\left(\delta_m^t - \delta_{m'}^t\right) + F_{t_j}\left(\delta_l^t - \delta_{l'}^t\right)\right] \quad (10.b)$$

The forces - so do deformations - in (t, n) system are related to those in (x, y) system by the following transformation:

$$F_{t_i} = F_{x_i} \cos\theta + F_{y_i} \sin\theta \qquad F_{n_i} = -F_{x_i} \sin\theta + F_{y_i} \cos\theta \quad (11.a, b)$$

Raju [5] showed that the use of singular Q8 elements gives more accurate results than those related to non-singular Q8 ones. However, he used coarse mesh in his computations. Moreover, Henshell and Shaw [17] had concluded their work by declaring that special finite elements for crack tips are not necessary for plane stress/strain analysis. Hence, the author in this work has used fine mesh of Q8 element in computations of strain energy release rates.

SUMMARY OF THE CLASSICAL DISPLACEMENT-BASED FINITE ELEMENT METHOD

Basics of the classical displacement-based FEM are extensively explained in many reference books, [12-13]. In this section, main principals are briefly written. Interested reader should refer to the listed references. The horizontal and vertical displacements within Q8 element are:

$$u(x,y) = N_i u_i \qquad v(x,y) = N_i v_i \qquad i = 1,2,\dots 8 \tag{12.a}$$

where u_i and v_i are nodal displacements in x- and y- directions respectively, N_i are shape function.

Cartesian components strain vector $\boldsymbol{\varepsilon} = [\varepsilon_x \quad \varepsilon_y \quad \gamma_{xy}]^T$ are:

$$\varepsilon_x = \frac{\partial u}{\partial x} \qquad \varepsilon_y = \frac{\partial v}{\partial y} \qquad \gamma_{xy} = \frac{\partial u}{\partial y} + \frac{\partial v}{\partial x} \tag{12.b}$$

Cartesian components of stress vector are:

$$\boldsymbol{\sigma} = \mathbf{D}\boldsymbol{\varepsilon} = \mathbf{DBd} \tag{12.c}$$

Where $\mathbf{B}$ is the strain-displacement matrix. The element stiffness matrix, force vectors in case of surface traction; T_y, and element equilibrium equation are calculated according to:

$$\mathbf{K} = \int_V \mathbf{B}^T\mathbf{DB}\, dV \qquad \mathbf{F} = \int_S \mathbf{N}^T \begin{Bmatrix} 0 \\ T_y \end{Bmatrix} dS \qquad \mathbf{Kd} = \mathbf{F} \tag{12.d}$$

Where V is element's volume, and S is element's surface where traction is applied Evaluations $(12.d_{1,2})$ are formed numerically using 2×2 Gauss numerical integration rule. Locations of gauss points are shown in figure 4.b.

VALIDATION OF SIF RESULTS

This section aims to verify the computations of SIFs in case of the single edge notch test and three-point bend test specimens. The analytical values of $K_I^{analytical}$ are calculated according to Tada et. al. [18]. Percentage errors in computation of K_I are calculated according to the following equation:

$$e_{K_I} = \frac{K_I - K_I^{analytic}}{K_I^{analytic}} \times 100 \tag{13}$$

Specimens investigated in this work are made of high-strength steel; AISI 4340 steel. Mechanical properties of steel 4340 are listed in Table 1 [16]. Units are selected to be

a Newton $[N]$ for the force and millimeters $[mm]$ for the length. The following rules in selecting numerical values of loads and crack length are considered: (1) A specimen is loaded under its yield point to avoid the formation of plastic strains. So, the principals of linear elastic fracture mechanics (LEFM) are applied. (2) A crack has a length that exceeds the critical crack length a_c. So, the crack would propagate spontaneously as soon as the fracture toughness of the material is exceeded. (3) A load is selected to overcome material's fracture toughness.

Table 1. Mechanical properties of AISI 4340 steel.

$E, \left[\frac{N}{mm^2}\right]$	ν	$\sigma_{yp}, \left[\frac{N}{mm^2}\right]$	$K_{I_c}, \left[\frac{N}{mm^{3/2}}\right]$	$a_c, [mm]$
210000	0.3	860	3130.655	16.8

Single Edge Notch Test Specimen

Figure 5(a) shows dimensions and boundary conditions of the single edge notch test specimen. Crack length is $20\ mm$. Specimen's width and length are $70\,mm$ and $140\,mm$, respectively. Nodes of the bottom surface are completely constrained. Top surface nodes are under vertical tensile traction of $T_y = 480\frac{N}{mm^2}$. Left and right surfaces are traction-free and they are not constrained.

The deformed finite element mesh used in the present work (600 elements and 1579 nodes) and in the ANSYS APDL program (2110 elements and 6584 nodes) are shown in Fig. 5(b) and (c) respectively. Results of K_I are listed in Table 2. ANSYS's result is closer to the analytical one, however, its mesh is denser than that is used in the present work. Due to unsymmetry of the single edge carcked specimen, a sliding mode SIF appears in FEM computations; i.e. $K_{II} = -15.2734\ \left[N/mm^{\frac{3}{2}}\right]$ obtained from the present work and $K_{II} = -23.1047\left[N/mm^{\frac{3}{2}}\right]$ obtained from ANSYS APDL. This effect doesn't appear in the analytical solution found in [18] page 52.

Table 2 Validation of $K_I, \left[N/mm^{\frac{3}{2}}\right]$ results.

	Single edge notch	$e_{K_I}, \%$	**Three - point bend**	$e_{K_I}, \%$
Analytical	6.1084×10^3		3.3292×10^3	
ANSYS	6.0781×10^3	-0.4982	3.1633×10^3	-5.2524
Present Work	6.0714×10^3	-0.6060	3.1444×10^3	-5.5504

The Three – Point Bend Test Specimen

Dimensions of the three-point bend test specimen are shown in Fig. 6(a). Specimen's length and height are $280\ mm$ and $70\ mm$, respectively. The crack length is $20\,mm$; it is located at the mid length of the specimen. The specimen is hinged to right and left rigid supports at the mid height of each surface. A point vertical load $P_y = -4900\ [N]$

is applied at the mid length of the top surface as shown in the figure. The bottom surface is a traction-free and is not constrained.

Mesh densities are 630 elements with 1641 nodes in the present work, Fig. 6(b), and 7356 elements with 22650 nodes in ANSYS APDL, Fig. 6(c). Results of K_I calculated in the present work and ANSYS program are very close to the analytical one, Table 2. However, ANSYS required denser mesh to reach such accuracy.

PROPAGATION OF AN INCLINED EDGE CRACK IN A PLATE UNDER TENSILE TRACTION

Specimen of the inclined crack is shown in Fig. 7(a). Results of crack characteristics are listed in Table 3. According to equation (4.b), the equivalent SIF is $K_{eq} = 5.205 \times 10^3\ [N/m^{\frac{3}{2}}]$; this value violates the condition of equation (5.a). Hence, the crack starts to propagate at the angle $\theta_C = -26.193°$, as shown in Fig. 7. According to equation (7.c), the equivalent SIF of the propagating is $K_I^{\theta_C} = 5.5 \times 10^3\ [N/m^{\frac{3}{2}}]$, which violates the condition of equation (8). Hence, the crack continues to propagate until it separates the specimen completely.

Table 3. Numerical results of crack characteristics in case of the inclined edge crack specimen.

$G_I, [N/mm]$	$G_{II}, [N/mm]$	$K_I, \left[N/mm^{\frac{3}{2}}\right]$	$K_{II}, \left[N/mm^{\frac{3}{2}}\right]$	θ_c
110	7.48	5.036×10^3	1.314×10^3	$-26.193°$

SHIFTED CRACK IN A BEAM UNDER THREE-POINT BENDING TEST SPECIMEN

This section deals with the propagation of cracked John and Shah beam problem presented in the work of T. Rabczuk and T. Belytscho [15] and Gonzalo Ruiz et. al. [19]. Figure 8(a) illustrates the geometry of the shifted cracked beam under three -point bending test. The crack is shifted by $50.08\ mm$ from the left support. The mechanical properties of the beam's material are $E = 29000\ [N/mm^2]$ and $G_{Tc} = 0.0311\ [N/mm]$. In the present work, the applied force is $P_y = 350\ [N]$ selected to cause crack energy release of $G_T = 0.0540\ [N/mm]$ that exceeds the critical value of fracture toughness of the beam. The results of crack deflection angle calculated in the present work and by ANSYS APDL are listed in Table 4. Present work mesh and ANSYS' one are shown in Fig. 8(a) and (b) respectively.

Table 4 Calculation of crack deflection angle for John and Shah cracked beam problem.

	T. Rabczuk and T. Belytscho [15], Fig. 9(a)	Present work.	ANSYS
θ_C	$30°$	$29.76°$	$26.14°$

COMPARISON WITH EXPERIMENTAL WORK

This section compares the crack pattern in the experimental work of John and Shah that presented in [15] and the simulation results of the present work and ANSYS APDL commercial program. Figure 9(b) illustrates the crack pattern of the shifted crack beam under the quasi-static loading conditions. The observed angle of crack deflection is about $30°$ which is very close to that calculated in the present work ($29.76°$), Table 4. In addition, the observed crack pattern is very close to simulation results that presented in this work, Fig. 10.

Figure 11 illustrates simulation results of ANSYS APDL program of John and Shah cracked beam problem. To simulate crack propagation in the framework of ANSYS technology, the predefined crack path is meshed with interfacial elements (INTER202). Such elements are conformed to solid four-noded isoparametric structural elements (PLANE182). If the higher order interfacial elements such as (INTER203), which are conformed to eight-noded isoparametric structural elements (PLANE183), are used, a cohesive zone model that controlling crack propagation must be used. The problem of the cohesive zone model is not considered in this work.

CONCLUSION

This work presents the following conclusions: (1) Using fine structured mesh of non-singular Q8 elements around the crack tip gives accurate values of crack characteristics using the VCCT. (2) Cracks, propagating in an elastic and isotropic medium neither deviate, bifurcate nor arrest. (3) Creation of a new pair of crack faces can be simulated by duplication of the nodes behind the advancing crack tip and performing the corresponding changes in the element connectivity matrix. Simulation process should be accompanied with continuous update of nodal coordinates, stiffness matrix and load vector.

REFERENCES

[1] J. Jung, J. Ahmad and M.F. Kanninen, “Finite Element Analysis of Dynamic Crack Propagation”, Failure Prevention and Reliability Conf., Hartford, (1981).

[2] Nicolas Moes, John Dolbow, and Ted Belytschko, “A Finite Element Method For Crack Growth Without Remeshing”, Int. J. Numer. Meth. Engng., 46, pp. 131-150, (1999).

[3] T. Nishioka and S.N. Alturi, ”Numerical Modeling of Dynamic Crcak Propagation in Finite Bodies, by Moving Singular Elements; Part 1: Formulation”, Transaction of the ASME, Vol. 47, pp. 570-576, (1980).

[4] Brain Lawn, “Fracture of Brittle Solids”, 2nd ed., Cambridge Unv. Press, (1993).

[5] I. S. Raju, “Calculation of Strain Energy Release Rates with Higher Order and Singular Finite Elements”, Engng Frac. Mech., Vol. 28, 3, pp. 251-274, (1987).

[6] T. Belytschko and T. Black, “Elastic Crack Growth in Finite Elements with Minimal Remeshing”, Int. J. Numer. Meth. Engng., 45, pp. 601-620, (1999).

[7] N. Sukumar and J.H. Prevost, “Modeling Quasi-Static Crack Growth with The Extended Finite Element Method. Part I: Computer Implementation”, International Journal of Solids and Structures, 40, pp. 7513–7537, (2003).

[8] Reeder J. R., "A Bilinear Failure Criterion for Mixed-Mode Delamination," Composite Materials: Testing and Design, Vol. 11th, ASTM STP 1206, pp. 303-322, (1993).
[9] M.A. Meggiolaro, A.C.O. Miranda, J.T.P. Castro, L.F. Martha, “Stress Intensity Factor Equations for Branched Crack Growth”, Engineering Fracture Mechanics, 72, pp. 2647-2671, (2005).
[10] Ronald Krueger, ”Virtual Crack Closure Technique: History, Approach, and Applications”, Appl Mech Rev, Vol 57, No 2, pp. 109-143, (2004).
[11] Anderson T.L., “Fracture Mechanics - Fundamentals and Applications”, 3rd ed., Boca Raton: CRC, 2005.
[12] E. Onate, Structural Analysis with the Finite Element Method. Linear Statics. Volume 1. Basis and Solids, Springer, 2009.
[13] O.C. Zienkiewicz, R.L. Taylor, and J.Z. Zhu, “The Finite Element Method: Its Basis and Fundamentals”, 7th ed., Butterworth-Heinemann, (2013).
[14] http://www.automesh2d.com/default.htm.
[15] T. Rabczuk and T. Belytscho, “An Adaptive Continuum / Discrete Crack Approach for Meshfree Particle Methods”, Latin American Journal of Solids and Structures, 1, pp. 141-166, (2003).
[16] K. Lingaiah, “Machine Design Databook”, 2nd ed., MacGraw-Hill, (2003).
[17] Henshell RD, Shaw KG, “Crack Tip Finite Elements Are Unnecessary”, Int. J. for Numerical Methods in Engng, Vol. 9, pp. 495 – 507, (1975).
[18] Tada H., Paris P.C., and Irwin G.R., The Stress Analysis of Cracks Handbook, 3rd ed., ASME Press, New York, (2000).
[19] Gonzalo Ruiz, Anna Pandolfi and Michael Ortiz, “Three-Dimensional Cohesive Modeling of Dynamic Mixed-Mode Fracture”, Int. J. Numer. Meth. Engng., 52, pp 97–120, (2001).

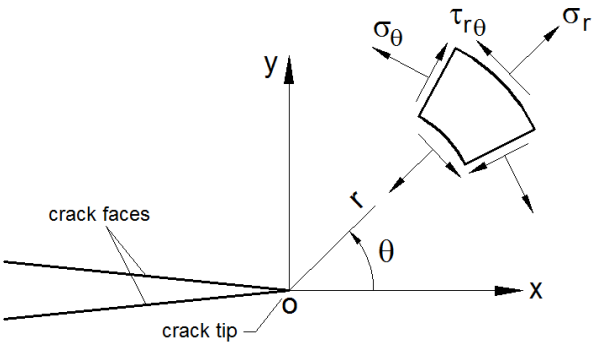

Fig. 1. Polar stress fields around a crack tip.

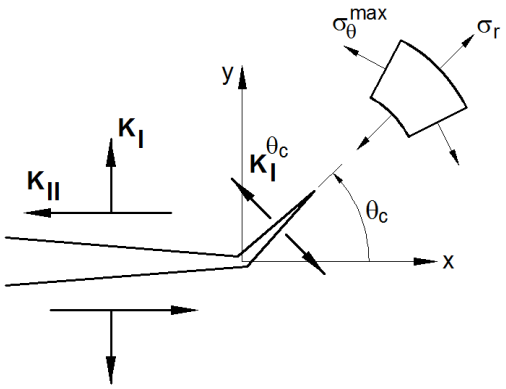

Fig. 2. The crack deflection angle

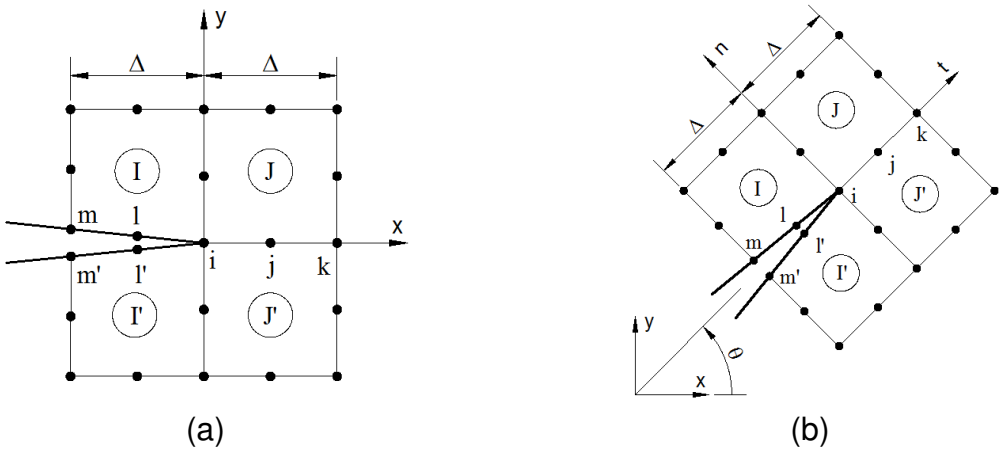

(a) (b)

Fig. 3. Arrangements of Q8 elements around a crack tip in order to fulfill VCCT requirements in case of (a) a horizontal and (b) an inclined crack.

(a) (b)

Fig. 4. Isoparametric quadrilateral Q8 element in (a) (x, y) and (b) normalized (ξ, η) coordinates system and location of Gauss points p_i.

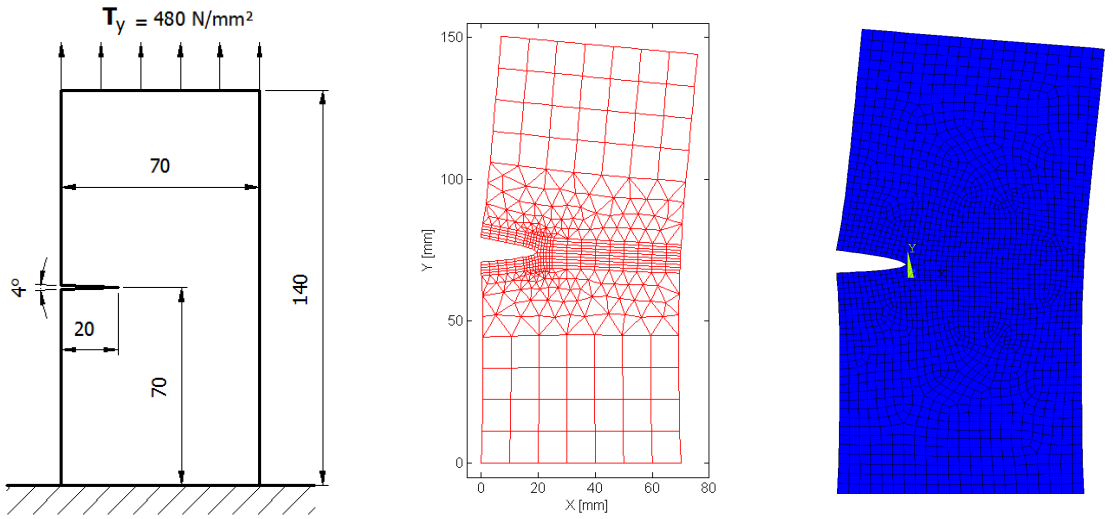

(a) (b) (c)

Fig. 5. (a) Single edge notch test specimen model. Deformed FE mesh; (b) Present work and (c) ANSYS. Deformations are multiplied by 20 for illustrative purposes.

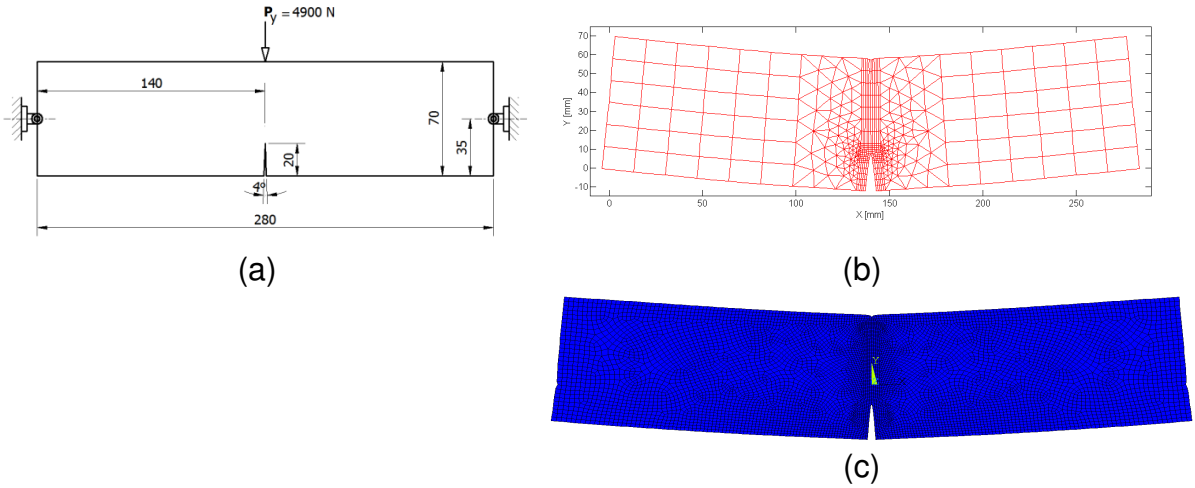

(a) (b)

(c)

Fig. 6. (a) The three – point bend test specimen; Deformed FE mesh (b) Present work and (c) ANSYS. Deformations are multiplies by 20 for illustration purposes.

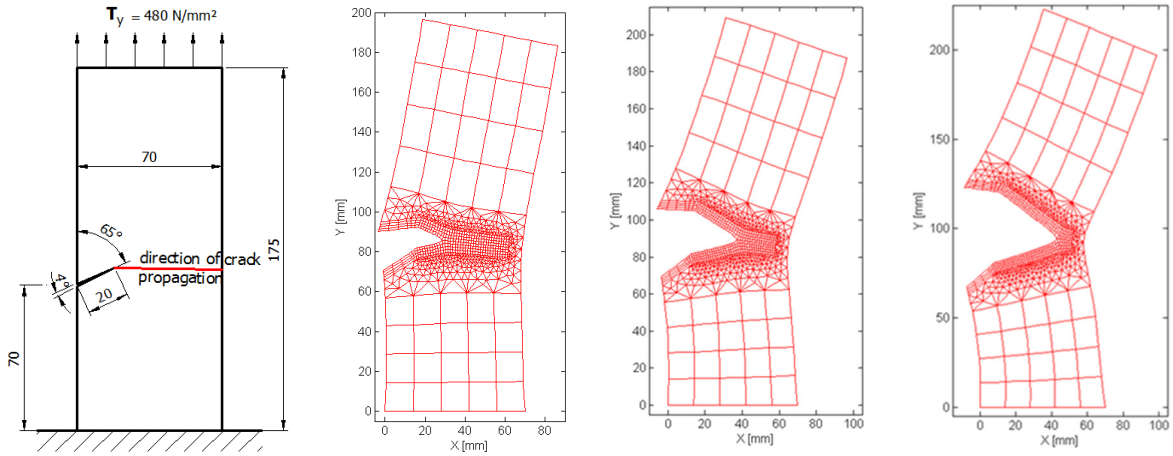

(a) (b) (c) (d)

Fig. 7 (a) Direction of crack propagation. Propagated crack at the (b) 10th, 20th, and 30th simulation loop.

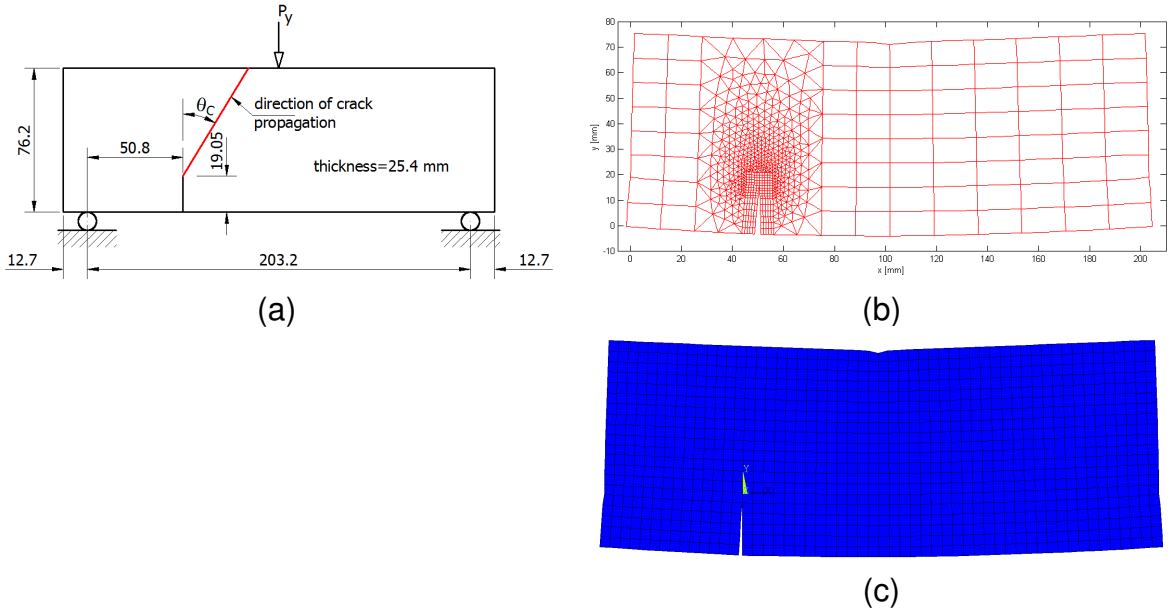

(a) (b)

(c)

Fig. 8 (a) John and Shah cracked beam problem. Deformed FE mesh; (b) Present work and (c) ANSYS. Deformations are multiplies by 50 for illustration purposes.

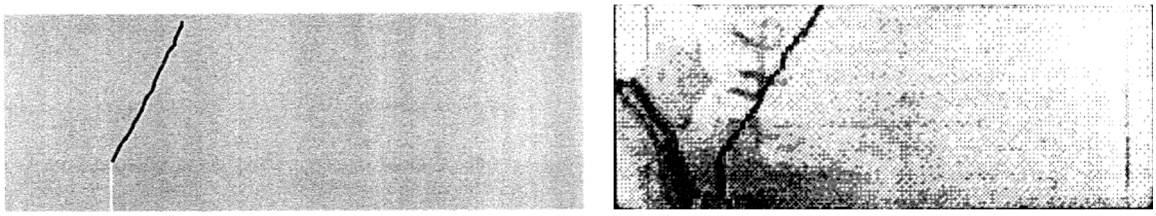

(a) (b)

Fig. 9. Work of Rabczuk and Belytscho in case of quasi-static loading; (a) simulation and (b) experiment.

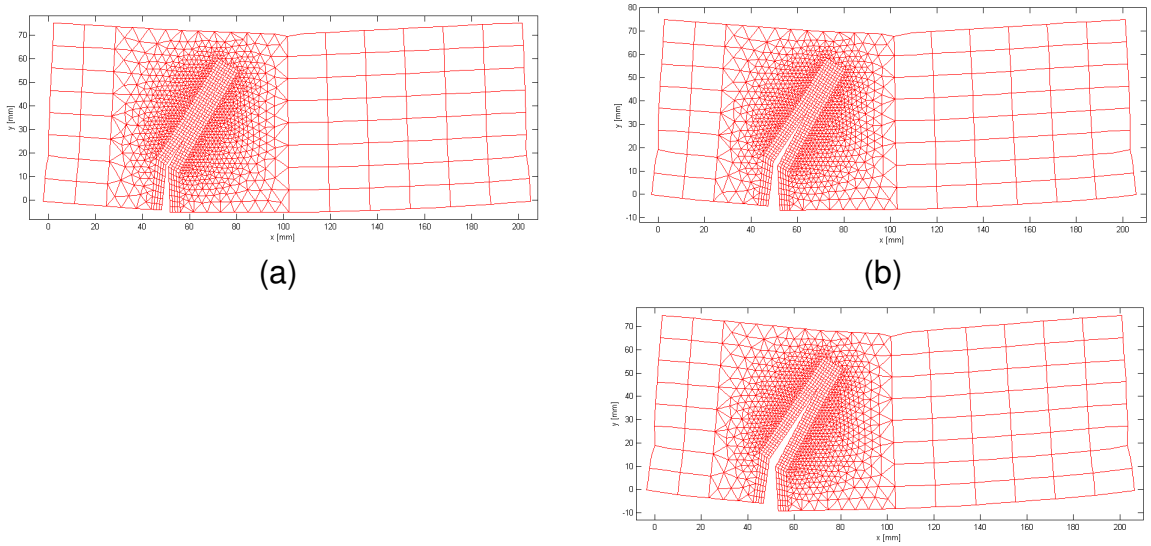

(a) (b)

(c)

Fig. 10. Present work simulation of John and Shah cracked beam problem at; (a) 10th loop, (b) 20th loop and (c) 30th loop. Deformations are multiplied by 50 for illustrative purposes.

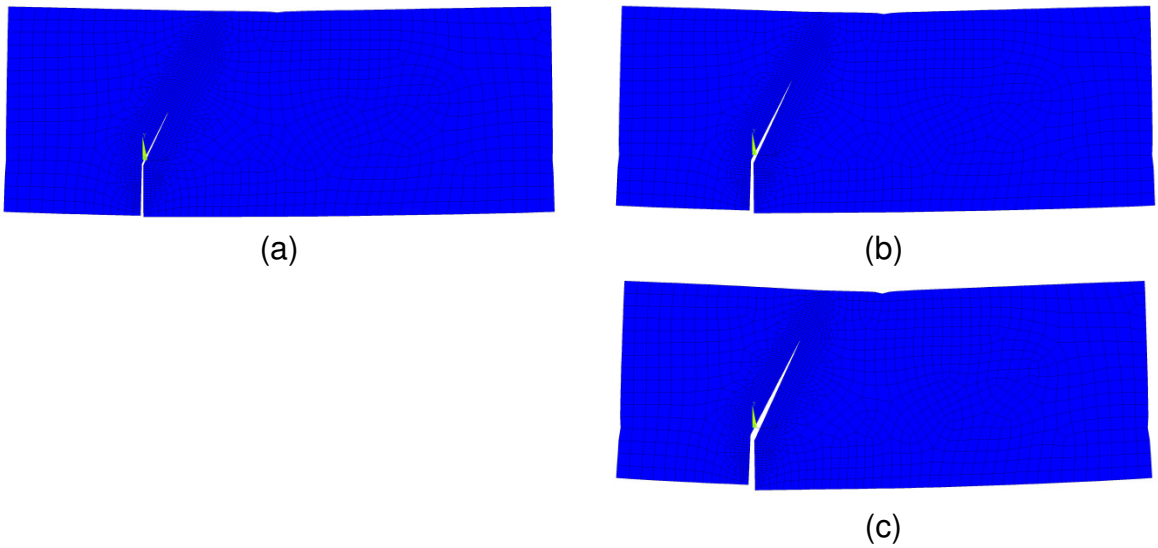

Fig. 11. ANSYS APDL simulation of John and Shah cracked beam problem at; (a) 250th, (b) 400th and (c) 600th sub-step of ANSYS computations. Deformations are multiplied by 50 for illustrative purposes.